



# Turbulent heat transfer in tubular heat exchangers with twisted tape

R. Hosseinejad<sup>1</sup> · M. Hosseini<sup>1</sup> · M. Farhadi<sup>2</sup>

Received: 14 February 2018 / Accepted: 21 May 2018 / Published online: 23 June 2018  
© Akadémiai Kiadó, Budapest, Hungary 2018

## Abstract

Enhancing heat transfer in heat exchangers has gained attention of researchers for many years because of reduction in costs of generating heat exchanger. Application of improved tubes is one way of increasing heat transfer. In the present study, the turbulent flow in tubular heat exchangers with two twisted tapes was numerically investigated. Constant input velocity and output pressure with non-slip conditions on the surface of the tape and the tube were also considered as the hydrodynamic boundary condition. In addition, the constant heat flow and heat resistance boundary conditions were also considered for the surface of the tube and the tape, respectively. The fluent software was applied to solve the governing differential equations. Results indicated that reducing the torsion ratio at constant Reynolds number with unaligned orientation of tapes increases the average Nusselt number. Results also demonstrated that in aligned orientation, performance enhancement is more compared to aligned orientation.

**Keywords** Turbulent flow · Heat exchanger · Twisted tape · Simulation · Thermal performance

## List of symbols

$D$	Pipe diameter (m)
$f$	Darcy friction factor (–)
TR	Torsion ratio (–)
$L$	Length of pipe (m)
$N_e$	Number of twists
$Nu$	Nusselt number
$t$	Thickness of the fin
$Pr$	Prandtl number
$P$	Step or length of twist
$w$	Width of the tape
$T$	Fluid temperature (K)
$Re$	Reynolds number

## Greek symbols

$\alpha$	Thermal diffusivity ( $\text{m}^2 \text{s}^{-1}$ )
$\mu$	Dynamic viscosity of nanofluid (Pa s)
$\rho$	Density ( $\text{kg m}^{-3}$ )
$\lambda$	Half twist

## Subscripts

i	Inner
o	Outer

## Introduction

Among all the equipment which are used for generation of rotational flow or secondary flow, twisted tape has gained specific attention due to good heat performance of these tapes in single-phase media and two-phase flow. In addition, these taps have desired flexibility in operation [1]. The presence of twisted tape leads to simultaneous increase in heat transfer coefficient and pressure drop. Due to simple design and operation of twisted tape, they have extensively been used for generation of rotational flow in liquids over the past few decades. The size of heat exchangers can be dramatically reduced when twisted tape is used to generate specified heat. Therefore, more equipment is provided with constant expenditure which is economically advantageous. Another benefit of using twisted tapes is their easy production and implementation in comparison with other rotational current generators [2].

In the past 60 years, researchers and engineers were trying to use tools to increase the turbulence intensity of mixtures and turbulent flow in order to achieve higher heat transfer [3]. Twisted tapes have high ability for increasing these parameters in heat transfer systems including steam

✉ R. Hosseinejad  
R.hosseinejad@nit.ac.ir

<sup>1</sup> Department of Mechanical, Islamic Azad University, Ghaemshahr Branch, Ghaemshahr, Mazandaran, Iran

<sup>2</sup> Department of Mechanical Engineering, Babol Noshirvani University of Technology, Babol, Iran

boilers, shell and tube heat exchangers and even simple radiators of cars.

In 1976, Manglik and Bergles [4] performed experimental investigations to increase the heat transfer in a tube with constant temperature surfaces. In this study, by inserting one twisted tape with torsion ratio of 3, 4.5 and 6 in the tube and application of water as the fluid, they came to the conclusion that for all three ratios, the heat transfer increased 1.3–1.5 times and the friction coefficient had also increased 2–3 times, compared to hollow tube. Their results indicated that the reduction of torsion ratio leads to higher heat transfer rate and pressure drop. Jafaryar et al. [5] investigated twisted tape with alternate axis effect on turbulent flow and forced convection heat transfer. They utilized single-phase model for nanofluid. Sheikholeslami et al. [6] presented the nanofluid turbulent convective flow in a circular duct with helical turbulators. Shadloo and Hadjadj [7] studied the Laminar-turbulent transition in supersonic boundary layers with surface heat transfer. Saha et al. [8] experimentally studied the effect of twisted tape with different length on heat transfer in the tube with constant temperature flux. Results indicated that shorter length tapes possessed better thermal performance in comparison with the long tape. Heat transfer and pressure drop encountered 1.6–2.5 times and 3–4.5 times increase, respectively.

Sheikholeslami et al. [9] investigated solidification of NEPCM by means of finite element method. Shadloo et al. [10] reported the statistical behavior of supersonic turbulent boundary layers with heat transfer in high Mach number. Sheikholeslami [11] utilized metallic fin to enhance the conduction heat transfer during solidification of phase change material. Sheikholeslami and Ghasemi [12] investigated thermal radiation effect on unsteady heat conduction of nanofluid. Goodarzi et al. [13] investigated the heat transfer and pressure drop of a counterflow corrugated plate heat exchanger using MWCNT-based nanofluid. Sheikholeslami et al. [14] studied heat transfer improvement and pressure drop during condensation of refrigerant-based nanofluid. Sheikholeslami and Shehzad [15] simulated ferrofluid flow in a porous media in existence of magnetic source. Goodarzi et al. [16] studied application of nitrogen-doped, graphene-based nanofluids for counterflow double-pipe heat exchanger. Sheikholeslami and Bhatti [17] investigated shape effects of nanoparticles on nanofluid forced convection in existence of Lorentz forces. Goodarzi et al. [18] studied nanofluid mixed convection in a shallow cavity using a two-phase mixture model. Recently, several articles have been published about various methods of heat transfer enhancement [19–67].

In this paper, effect of twisted tape on turbulent flow and heat transfer enhancement are demonstrated. The twisted

tape static mixer pioneered the motionless mixing industry. It is a cost-effective static mixer with moderate mixing performance capabilities. It is most suitable for use in small diameter turbulent and laminar flow applications where the mixing task is simple and where its characteristic features of low-pressure drop and an open geometric structure are best for the application. Effect of active parameters on flow style and variation of Nusselt number have been presented.

## Governing equations

In order to understand and discuss the properties of twisted tape, it is important to introduce the parameters which are used throughout this research paper.

### 1. Step or length of twist ( $P$ )

The length of twist which indicates the 360 angle in twisted tape is called the step or length of twist.

### 2. Number of twists ( $Ne$ )

The number of 360° twists in the twisted tape.

### 3. Reynolds number ( $Re$ )

The Reynolds number is defined as the one in the hollow tube.

$$Re = \frac{VD}{\nu} \quad (1)$$

In which  $V$  is velocity,  $D$  is the diameter of the tube and  $\nu$  is the kinetic viscosity described as follows:

$$\nu = \frac{\mu}{\rho} \quad (2)$$

where  $\mu$  and  $\rho$  are density and dynamic viscosity, respectively.

### 4. Half twist ( $\lambda$ )

The length of tube in which one twisted tape completed 180° rotation.

### 5. Torsion ratio (TR)

TR is known as the ratio of half twist to the width of the tape.

$$TR = \frac{\lambda}{W} \quad (3)$$

In which  $W$  is the width of the tape. The increase in heat transfer with the aid of twisted tape is extensively used in heat exchangers. The important effects caused by the presence of twisted tape are rotating flow which improves liquid mixing; the spiral rotation of the fluid effectively increases the length of flow path. In addition, barrier formation and separation of flow lines result in increased velocity in some areas of the flow [4].

In other words, the mechanisms of increased heat transfer by twisted tape can be described as follows:

- The effective flow lines in the current field and its velocity in the rotational flow (due to the presence of twisted tape) is more than the simple tube. This affects the heat transfer coefficient from two aspects:
- Volatility increased heat transfer
- Higher tangential velocity in the vicinity of tube walls.
- The secondary flow generated by twisted tape increases the flow mixing due to the rotational flow. The eccentric force which is produced by this secondary flow generates rotational flow on both sides of the twisted tape.
- The blade effect in twisted tape, in case when it is attached to the tube, can increase the surface of heat transfer. This increase is a function of contact area of the tape and tube and the other thermophysical properties of the tape and the tube.

As mentioned previously, turbulent flow is generally irregular and unpredictable. However, observation of fluid flow in this case indicates that this flow has fairly regular structures consisted of relatively large vortices in comparison with the flow. In other words, the flow is statistically stable. With this property, variables can be defined using Eq. (4):

$$\varnothing = \overline{\varnothing} + \varnothing' \tag{4}$$

where  $\overline{\varnothing}$  and  $\varnothing'$  terms represent the mean value and the volatility of the variable, respectively. The time average of  $\varnothing$  quantity is calculated using Eq. (5):

$$\int_0^{\Delta t} \varnothing(x_i, t) \lim_{\Delta t \rightarrow \infty} \frac{1}{\Delta t} dt = (x_i)\overline{\varnothing} \tag{5}$$

Reynolds considered the variables in the form of Eq. (4), inserting in flow equations and averaging the equations described the flow equations in terms of mean and volatility variables for the first time which is called Reynolds averaged equations [5].

$$\frac{\partial(\overline{u_i})}{\partial x_i} = 0 \tag{6}$$

$$\frac{\partial}{\partial x_j} (\overline{u_i u_j} + \overline{u_i' u_j'}) = \frac{1}{\rho} \left( -\frac{\partial \overline{p}}{\partial x_i} + \frac{\partial \overline{\tau_{ij}}}{\partial x_i} \right) \tag{7}$$

$$\frac{\partial}{\partial x_j} (\overline{u_j \varnothing} + \overline{u_j' \varnothing'}) = \frac{1}{\rho} \frac{\partial}{\partial x_j} \left( \Gamma \frac{\partial \overline{\varnothing}}{\partial x_j} \right) \tag{8}$$

where  $\overline{\tau_{ij}}$  elements are viscose mean stress tensor.

$$\overline{\tau_{ij}} = \mu \left( \frac{\partial \overline{u_i}}{\partial x_j} + \frac{\partial \overline{u_j}}{\partial x_i} \right) \tag{9}$$

These equations have almost the same structure as the fundamental mass, momentum and scalar conservations; however, the new equations are based on mean variables and the terms are actually representing the effect of turbulence which are added to these equations. The presence of turbulent terms, terms such as  $\overline{\rho u_i' u_j'}$  (Reynolds stresses) and  $\overline{\rho u_i' \varnothing'}$  (Scalar turbulent flux) in conservation equations means that these equations are not closed; in other words, the number of variables are higher than the number of equations. In order to close these equations, the new terms which are associated with turbulent flow should be modeled which leads to different turbulent models. Figure 1 and Table 1 show good agreement of presented code. Table 2 shows more detail of setting.

Nusselt number can be defined as:

$$Nu = \frac{h D_h}{k_{nf}} \tag{10}$$

### Results

It should be mentioned in this section that the torsion ratio is equal for all the simulations. In fact, the known torsion ratio in one case, determines the torsion ratio for both tapes. Therefore, in this section, two parameters of torsion ratio and Reynolds number are investigated. In Fig. 2, the 3-D flow lines in the center of the tube for aligned and unaligned orientation with torsion ratio of 4 are illustrated.

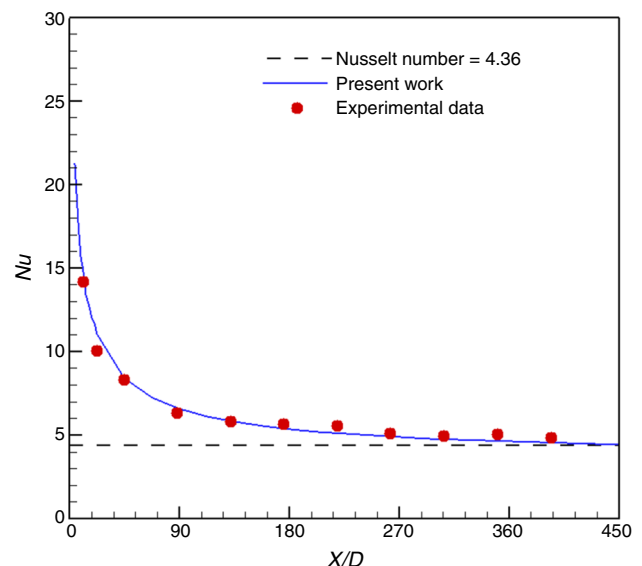


Fig. 1 Comparison of the results obtained for water in a horizontal pipe [67]

**Table 1** Comparison of average Nusselt number between present work and Aminossadati et al. [66]

$Re$	$\phi$	Aminossadati et al. [66]	Present work
10	0.01	1.486	1.508
10	0.04	1.580	1.569
500	0.01	7.330	7.330
500	0.04	8.136	8.136

In Fig. 3, the secondary flow generated on the twisting tapes in the tube with torsion ratio of 4 with different Reynolds numbers is shown.

As shown in Fig. 3, when Reynolds number is changed, no specific change occurs in the flow regime. This is while two rotational regions formed around each tape, in sections of the tube which the two tapes become closer, only one rotational region formed between the two tapes.

In Fig. 4, the generated secondary flow in some parts at Reynolds number of 20,000 and torsion ratio of 3.25 at aligned and unaligned orientations is illustrated. In can be seen that at unaligned orientation, one distinct rotational region formed around each tape does not interact with the other rotational region.

In this section, the effect of torsion ratio on heat transfer and specifically the Nusslet number was investigated. In the following figure, the obtained Nusselt number from performed simulations for different torsion ratios is indicated.

As illustrated in the figure, at constant Reynolds number, the Nusselt number increases with the reduction in torsion ratio. This is due to the increased intensity of the rotating flow in lower torsion ratios. In other words, at given distance of tube length, the fluid goes through a longer path (Fig. 5).

In addition, the generated secondary flow itself increases the rate of heat transfer. This increase in Nusselt number for higher Reynolds numbers is significantly higher. Finally, it should be considered that increase in Nusselt number with decreasing torsion ratio is comparatively higher when changed from 3.25 to 2.5 than in case of 4–3.25. However, the numerical value of this increase is

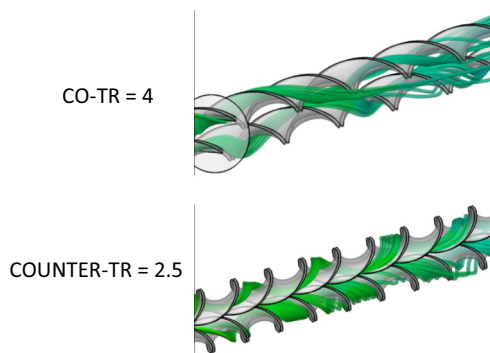


**Fig. 2** 3-D flow lines in two different conditions of torsion ratio and torsion orientation

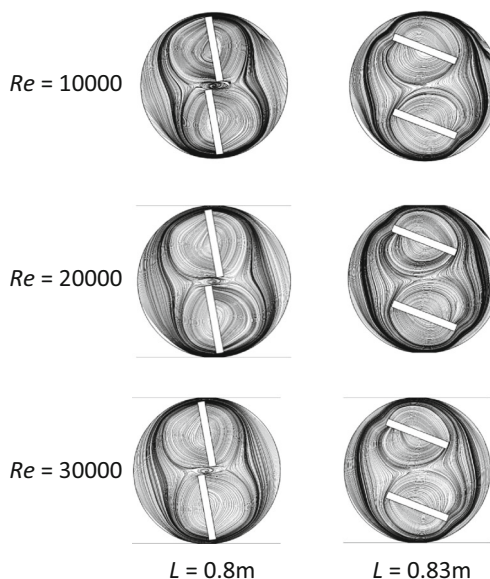


**Fig. 3** Secondary flow for different Reynolds numbers  $t$  torsion ratio of 4 at aligned orientation

evident and will be discussed in terms of percentage of increase in the following section. Figure 6 indicates the effect of the increase in torsion ratio on Nusslet number for unaligned orientation.

The obtained results on the increasing trend of heat transfer at aligned and unaligned orientation were similar. However, at unaligned orientation, the increase in heat

**Table 2** Solver setting of ANSYS FLUENT

Solver	<i>Pressure-based, steady</i>	
Viscous model	<i>K – ε, RNG, enhanced wall treatment</i>	
Solution methods	Pressure–velocity coupling	<i>SIMPLE</i>
	Gradient	<i>Green-Gauss node based</i>
	Pressure	<i>Standard</i>
Spatial discretization	Momentum	<i>Second-order upwind</i>
	Turbulent kinetic energy	<i>Second-order upwind</i>
	Turbulent dissipation rate	<i>Second-order upwind</i>

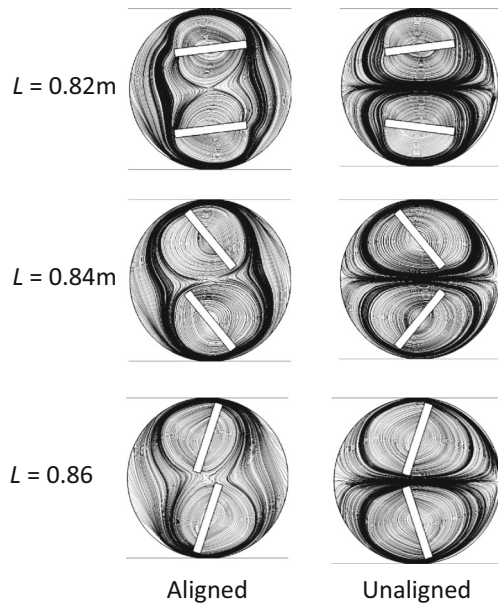


Fig. 4 Generated secondary flow at Reynolds number of 20,000 and torsion ratio of 3.25 for three different parts of the tube at aligned and unaligned orientations

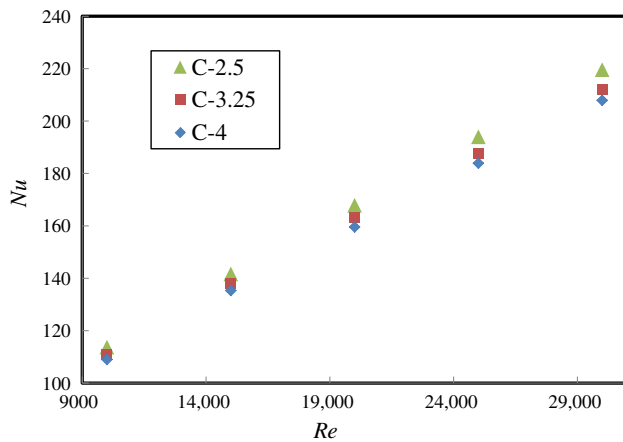


Fig. 5 Nusselt number with changing Reynolds number and different torsion ratios at aligned orientation

transfer at constant Reynolds number is higher for a decrease of 4–3.25 in torsion ratio in comparison with the Nusselt number obtained for decreased torsion ratio of 3.25–2.5. Comparison of the unaligned orientation of twisted tapes in increasing the heat transfer at different torsion ratios is investigated in this section. In the following figures, the variation of Nusselt number for different Reynolds numbers at aligned and unaligned orientations in each of the investigated three torsion ratios is compared (Fig. 7).

As can be seen, the Nusselt number increases with increase in unaligned orientation of the tape. This is physically logical because at unaligned orientation, two

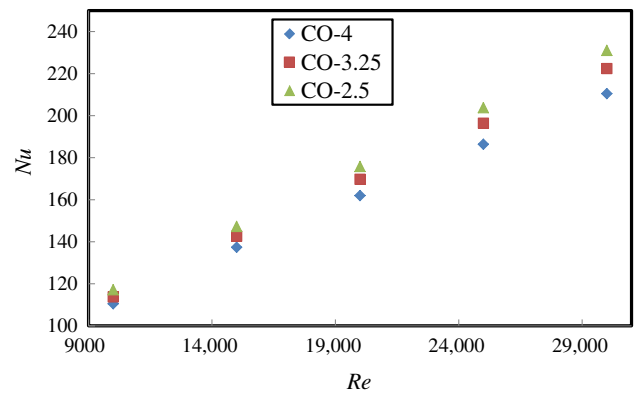


Fig. 6 Nusselt numbers with variation of Reynolds number at different torsion ratios and unaligned orientation

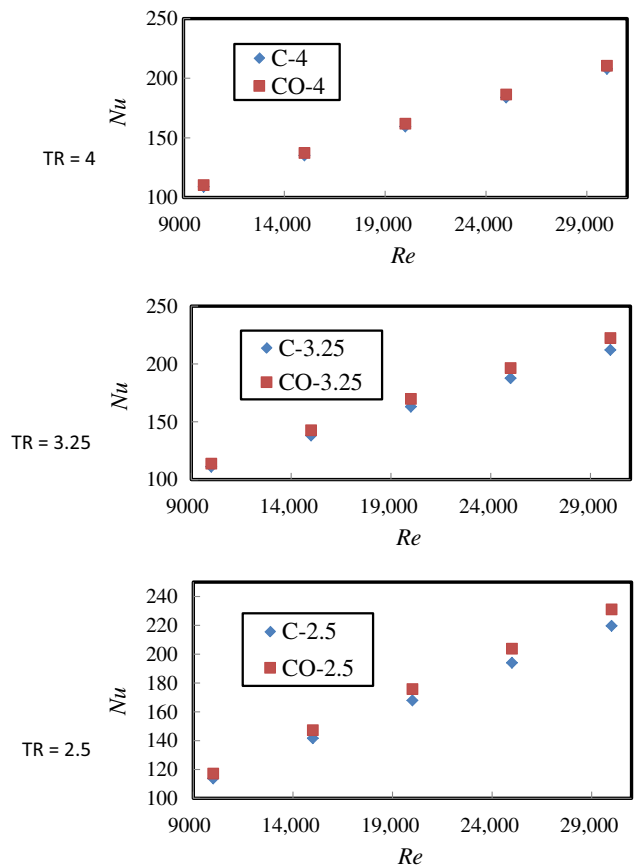


Fig. 7 Variation of Nusselt number with Reynolds number at three torsion ratios in aligned and unaligned orientations

tapes were very close at some points and therefore higher mixing of flow is observed which is ultimately effective in increasing the heat transfer. What should be mentioned here is that the increase in heat transfer at unaligned orientation of tapes was not significant at torsion ratio of 4 and is approximately equal for the other two torsion ratios.

## Conclusions

In the present study, turbulent water flow in tubular heat exchangers with twisted tapes was investigated. In order to simulate the turbulent flow  $K - \omega$ (SST) model was applied and Fluent software was used to solve the governing equations. Results indicated that numerical solution with the abovementioned method can effectively achieve results comparable to experimental results. Moreover, the obtained results were studied in the form of velocity contours, Nusselt number diagrams. Results demonstrated that two distinct rotational regions at unaligned orientation and two large rotational regions at aligned orientation were formed around the tubes. This can be explained based on 2-D flow lines at cross sections. The Nusselt number increases with the reduction of torsion ratio. This increase is higher for larger Reynolds numbers.

## References

- Johar G. Experimental studies on heat transfer augmentation using modified reduced width twisted tapes as inserts for tube side flow of liquids. BSc thesis, National Institute of Technology, Rourkela, India; 2010.
- Agarwal SK, Rao MR. Heat transfer augmentation for flow of viscous liquid in circular tubes using twisted tape inserts. *Int J Heat Mass Transf.* 1996;99:3547–57.
- Dewan A, Mahanta P, Sumithraju K, Kumar PS. Review of passive heat transfer augmentation techniques. *Proc Inst Mech Eng A J Power Energy.* 2004;218:509–27.
- Manglik RM, Bergles AE. Heat transfer and pressure drop correlations for twisted-tape inserts in isothermal tubes: part II—transit ion and turbulent flows. *J Heat Transf.* 1993;115:890–6.
- Jafaryar M, Sheikholeslami M, Li Z, Moradi R. Nanofluid turbulent flow in a pipe under the effect of twisted tape with alternate axis. *J Therm Anal Calorim.* 2018. <https://doi.org/10.1007/s10973-018-7093-2>.
- Sheikholeslami M, Jafaryar M, Li Z. Nanofluid turbulent convective flow in a circular duct with helical turbulators considering CuO nanoparticles. *Int J Heat Mass Transf.* 2018;124:980–9.
- Shadloo MS, Hadjadj A. Laminar-turbulent transition in supersonic boundary layers with surface heat transfer: a numerical study. *Numer Heat Transf Part A Appl.* 2017. <https://doi.org/10.1080/10407782.2017.1353380>.
- Saha SK, Gaitonde UN, Date AW. Heat transfer and pressure drop characteristics of laminar flow in a circular tube fitted with regularly spaced twisted-tape elements. *Exp Thermal Fluid Sci.* 1989;2(3):310–22.
- Sheikholeslami M. Numerical simulation for solidification in a LHTESS by means of nano-enhanced PCM. *J Taiwan Inst Chem Eng.* 2018. <https://doi.org/10.1016/j.jtice.2018.03.013>.
- Shadloo MS, Hadjadj A, Hussain F. Statistical behavior of supersonic turbulent boundary layers with heat transfer at  $M_\infty = 2$ . *Int J Heat Fluid Flow.* 2015;53:113–34.
- Sheikholeslami M. Numerical modeling of nano enhanced PCM solidification in an enclosure with metallic fin. *J Mol Liq.* 2018;259:424–38.
- Sheikholeslami M, Ghasemi A. Solidification heat transfer of nanofluid in existence of thermal radiation by means of FEM. *Int J Heat Mass Transf.* 2018;123:418–31.
- Goodarzi M, Amiri A, Goodarzi MS, Safaei MR, Dahari M. Investigation of heat transfer and pressure drop of a counter flow corrugated plate heat exchanger using MWCNT based nanofluids. *Int Commun Heat Mass Transfer.* 2015;66:172–9.
- Sheikholeslami M, Darzi M, Sadoughi MK. Heat transfer improvement and pressure drop during condensation of refrigerant-based nanofluid; an experimental procedure. *Int J Heat Mass Transf.* 2018;122:643–50.
- Sheikholeslami M, Shehzad SA. Numerical analysis of  $Fe_3O_4-H_2O$  nanofluid flow in permeable media under the effect of external magnetic source. *Int J Heat Mass Transf.* 2018;118:182–92.
- Goodarzi M, Kherbeet AS, Afrand M, Sadeghinezhad E. Investigation of heat transfer performance and friction factor of a counter-flow double-pipe heat exchanger using nitrogen-doped, graphene-based nanofluids. *Int Commun Heat Mass Transfer.* 2016;76:16–23.
- Sheikholeslami M, Bhatti MM. Forced convection of nanofluid in presence of constant magnetic field considering shape effects of nanoparticles. *Int J Heat Mass Transf.* 2017;111:1039–49.
- Goodarzi M, Safaei MR, Vafai K, Ahmadi G. Investigation of nanofluid mixed convection in a shallow cavity using a two-phase mixture model. *Int J Therm Sci.* 2014;75:204–20.
- Safaei MR, Ahmadi G, Goodarzi MS, Shadloo MS, Goshayeshi HR, Dahari M. Heat transfer and pressure drop in fully developed turbulent flow of graphene nanoplatelets-silver/water nanofluids. *Fluids.* 2016;1(3):1–20.
- Alipour H, Karimipour A, Safaei MR, Semirovi DT, Akbari OA. Influence of T-semi attached rib on turbulent flow and heat transfer parameters of a silver-water nanofluid with different volume fractions in a three-dimensional trapezoidal microchannel. *Physica E.* 2017;88:60–76.
- Sheikholeslami M, Sadoughi MK. Simulation of CuO–water nanofluid heat transfer enhancement in presence of melting surface. *Int J Heat Mass Transf.* 2018;116:909–19.
- Sheikholeslami M, Rokni HB. Simulation of nanofluid heat transfer in presence of magnetic field: a review. *Int J Heat Mass Transf.* 2017;115:1203–33.
- Sheikholeslami M, Seyednezhad M. Lattice Boltzmann method simulation for CuO-water nanofluid flow in a porous enclosure with hot obstacle. *J Mol Liq.* 2017;243:249–56.
- Sheikholeslami M, Hayat T, Alsaedi A. On simulation of nanofluid radiation and natural convection in an enclosure with elliptical cylinders. *Int J Heat Mass Transf.* 2017;115:981–91.
- Sheikholeslami M, Shehzad SA. CVFEM for influence of external magnetic source on  $Fe_3O_4-H_2O$  nanofluid behavior in a permeable cavity considering shape effect. *Int J Heat Mass Transf.* 2017;115:180–91.
- Sheikholeslami M, Seyednezhad M. Nanofluid heat transfer in a permeable enclosure in presence of variable magnetic field by means of CVFEM. *Int J Heat Mass Transf.* 2017;114:1169–80.
- Sheikholeslami M. Magnetic field influence on CuO– $H_2O$  nanofluid convective flow in a permeable cavity considering various shapes for nanoparticles. *Int J Hydrogen Energy.* 2017;42:19611–21.
- Sheikholeslami M, Shehzad SA. Magnetohydrodynamic nanofluid convective flow in a porous enclosure by means of LBM. *Int J Heat Mass Transf.* 2017;113:796–805.
- Sheikholeslami M, Sadoughi M. Mesoscopic method for MHD nanofluid flow inside a porous cavity considering various shapes of nanoparticles. *Int J Heat Mass Transf.* 2017;113:106–14.

30. Sheikholeslami M. Lattice Boltzmann method simulation of MHD non-Darcy nanofluid free convection. *Phys B*. 2017;516:55–71.
31. Sheikholeslami M. Influence of magnetic field on nanofluid free convection in an open porous cavity by means of Lattice Boltzmann method. *J Mol Liq*. 2017;234:364–74.
32. Sheikholeslami M. Magnetohydrodynamic nanofluid forced convection in a porous lid driven cubic cavity using Lattice Boltzmann method. *J Mol Liq*. 2017;231:555–65.
33. Sheikholeslami M, Shehzad SA. Thermal radiation of ferrofluid in existence of Lorentz forces considering variable viscosity. *Int J Heat Mass Transf*. 2017;109:82–92.
34. Sheikholeslami M. Magnetic field influence on nanofluid thermal radiation in a cavity with tilted elliptic inner cylinder. *J Mol Liq*. 2017;229:137–47.
35. Sheikholeslami M. Numerical simulation of magnetic nanofluid natural convection in porous media. *Phys Lett A*. 2017;381:494–503.
36. Sheikholeslami M. Influence of Lorentz forces on nanofluid flow in a porous cylinder considering Darcy model. *J Mol Liq*. 2017;225:903–12.
37. Sheikholeslami M. Influence of coulomb forces on Fe<sub>3</sub>O<sub>4</sub>-H<sub>2</sub>O nanofluid thermal improvement. *Int J Hydrogen Energy*. 2017;42:821–9.
38. Jafaryar M, Sheikholeslami M, Li Z. CuO-water nanofluid flow and heat transfer in a heat exchanger tube with twisted tape turbulator. *Technol*. 2018;336:131–43.
39. Safaei MR (2016) Mathematical modeling for nanofluids simulation: a review of the latest works. In: Akbar NS, editor. *Modeling and simulation in engineering sciences*. InTech. <https://doi.org/10.5772/64154>.
40. Sheikholeslami M. Finite element method for PCM solidification in existence of CuO nanoparticles. *J Mol Liq*. 2018;265:347–55.
41. Rashidi S, Mahian O, Languri EM. Applications of nanofluids in condensing and evaporating systems. *J Therm Anal Calorim*. 2017. <https://doi.org/10.1007/s10973-017-6773-7>.
42. Sheikholeslami M, Shehzad SA. CVFEM simulation for nanofluid migration in a porous medium using Darcy model. *Int J Heat Mass Transf*. 2018;122:1264–71.
43. Sheikholeslami M, Rokni HB. CVFEM for effect of Lorentz forces on nanofluid flow in a porous complex shaped enclosure by means of non-equilibrium model. *J Mol Liq*. 2018;254:446–62.
44. Sheikholeslami M, Rokni HB. Magnetic nanofluid flow and convective heat transfer in a porous cavity considering Brownian motion effects. *Phys Fluids*. 2018. <https://doi.org/10.1063/1.5012517>.
45. Heydari A, Akbari OA, Safaei MR, Derakhshani M, Alrashed AA, Mashayekhi R, Shabani GAS, Zarringhalam M, Nguyen TK. The effect of attack angle of triangular ribs on heat transfer of nanofluids in a microchannel. *J Therm Anal Calorim*. 2018;131(3):2893–912.
46. Brar LK, Singla G, Kaur N, Pandey OP. Thermal stability and structural properties of Ta nanopowder synthesized via simultaneous reduction of Ta<sub>2</sub>O<sub>5</sub> by hydrogen and carbon. *J Therm Anal Calorim*. 2015;119(1):453–60.
47. Akar S, Rashidi S, Esfahani JA. Second law of thermodynamic analysis for nanofluid turbulent flow around a rotating cylinder. *J Therm Anal Calorim*. 2017. <https://doi.org/10.1007/s10973-017-6907-y>.
48. Sheikholeslami M, Shehzad SA. Simulation of water based nanofluid convective flow inside a porous enclosure via non-equilibrium model. *Int J Heat Mass Transf*. 2018;120:1200–12.
49. Sheikholeslami M, Seyednezhad M. Simulation of nanofluid flow and natural convection in a porous media under the influence of electric field using CVFEM. *Int J Heat Mass Transf*. 2018;120:772–81.
50. Sheikholeslami M, Ghasemi A, Li Z, Shafee A, Saleem S. Influence of CuO nanoparticles on heat transfer behavior of PCM in solidification process considering radiative source term. *Int J Heat Mass Transf*. 2018;126:1252–64.
51. Sheikholeslami M. Numerical investigation of nanofluid free convection under the influence of electric field in a porous enclosure. *J Mol Liq*. 2018;249:1212–21.
52. Sheikholeslami M. CuO-water nanofluid flow due to magnetic field inside a porous media considering Brownian motion. *J Mol Liq*. 2018;249:921–9.
53. Sheikholeslami M, Rokni HB. Numerical simulation for impact of Coulomb force on nanofluid heat transfer in a porous enclosure in presence of thermal radiation. *Int J Heat Mass Transf*. 2018;118:823–31.
54. Sheikholeslami M. Numerical investigation for CuO-H<sub>2</sub>O nanofluid flow in a porous channel with magnetic field using mesoscopic method. *J Mol Liq*. 2018;249:739–46.
55. Safaei MR, Safdari Shadloo M, Goodarzi MS, Hadjadj A, Goshayeshi HR, Afrand M, Kazi SN. A survey on experimental and numerical studies of convection heat transfer of nanofluids inside closed conduits. *Adv Mech Eng*. 2016;8(10):1–14.
56. Sheikholeslami M, Shehzad SA, Abbasi FM, Li Z. Nanofluid flow and forced convection heat transfer due to Lorentz forces in a porous lid driven cubic enclosure with hot obstacle. *Compt Methods Appl Mech Eng*. 2018;338:491–505.
57. Sheikholeslami M, Hayat T, Muhammad T, Alsaedi A. MHD forced convection flow of nanofluid in a porous cavity with hot elliptic obstacle by means of Lattice Boltzmann method. *Int J Mech Sci*. 2018;135:532–40.
58. Sheikholeslami M, Hayat T, Alsaedi A. Numerical simulation for forced convection flow of MHD CuO-H<sub>2</sub>O nanofluid inside a cavity by means of LBM. *J Mol Liq*. 2018;249:941–8.
59. Sheikholeslami M. Solidification of NEPCM under the effect of magnetic field in a porous thermal energy storage enclosure using CuO nanoparticles. *J Mol Liq*. 2018;263:303–15.
60. Sheikholeslami M, Darzi M, Li Z. Experimental investigation for entropy generation and exergy loss of nano-refrigerant condensation process. *Int J Heat Mass Transf*. 2018;125:1087–95.
61. Sheikholeslami M, Shehzad SA, Li Z. Water based nanofluid free convection heat transfer in a three dimensional porous cavity with hot sphere obstacle in existence of Lorentz forces. *Int J Heat Mass Transf*. 2018;125:375–86.
62. Sheikholeslami M, Jafaryar M, Ganji DD, Li Z. Exergy loss analysis for nanofluid forced convection heat transfer in a pipe with modified turbulators. *J Mol Liq*. 2018;262:104–10.
63. Sheikholeslami M, Rokni HB. Melting heat transfer influence on nanofluid flow inside a cavity in existence of magnetic field. *Int J Heat Mass Transf*. 2017;114:517–26.
64. Karimipour A, D'Orazio A, Shadloo MS. The effects of different nano particles of Al<sub>2</sub>O<sub>3</sub> and Ag on the MHD nano fluid flow and heat transfer in a microchannel including slip velocity and temperature jump. *Physica E*. 2017;86:146–53.
65. Sheikholeslami M, Jafaryar M, Saleem S, Li Z, Shafee A, Jiang Y. Nanofluid heat transfer augmentation and exergy loss inside a pipe equipped with innovative turbulators. *Int J Heat Mass Transf*. 2018;126:156–63.
66. Aminossadati SM, Raisi A, Ghasemi B. Effects of magnetic field on nanofluid forced convection in a partially heated micro channel. *Int J Non-Linear Mech*. 2011;46:1373–82.
67. Kim D, Kwon Y, Cho Y, Li C, Cheong S, Hwang Y, Lee J, Hong D, Moona S. Convective heat transfer characteristics of nanofluids under laminar and turbulent flow conditions. *Curr Appl Phys*. 2009;9:119–23.